

1 **A genetic particle filter scheme for univariate data assimilation**
2 **into Noah-MP model across snow climates**

3 Yuanhong You^a, Chunlin Huang^b, Zuo Wang^a, Jinliang Hou^b, Ying Zhang^a, Peipei Xu^b

4
5 ^aCollege of Geography and Tourism, Anhui Normal University, Wuhu, 241002, China

6
7 ^bNorthwest Institute of Eco-Environment and Resources, Chinese Academy of Sciences, Lanzhou,
8 730000, China

9
10
11
12
13
14
15
16
17
18
19
20
21

Corresponding author: Chunlin Huang, Key Laboratory of Remote Sensing of Gansu Province,
Northwest Institute of Eco-Environment and Resources, Chinese Academy of Sciences, Lanzhou,
Gansu, 730000, China. (huangcl@lzb.ac.cn)

Submitted to: Hydrology and Earth System Sciences
May, 2023

22 **Abstract**

23 Accurate snowpack simulations are critical for regional hydrological predictions, snow
24 avalanche prevention, water resource management, and agricultural production, particularly during
25 the snow ablation period. Data assimilation methodologies are increasingly being applied for
26 operational purposes to reduce the uncertainty in snowpack simulations and enhance their predictive
27 capabilities. This study aims to investigate the feasibility of using Genetic Particle Filter (GPF) as a
28 snow data assimilation scheme designed to assimilate ground-based snow depth (SD) measurements
29 across different snow climates. We employed the default parameterization scheme combination
30 within the Noah-MP model as the model operator in the snow data assimilation system to evolve
31 snow variables and evaluated the assimilation performance of GPF using observational data from
32 sites with different snow climates. We also explored the impact of measurement frequency and
33 particle number on the filter updating of the snowpack state at different sites and the results of generic
34 resampling methods compared to the genetic algorithm used in the resampling process. Our results
35 demonstrate that GPF can be used as a snow data assimilation scheme to assimilate ground-based
36 measurements and obtain satisfactory assimilation performance across different snow climates. We
37 found that particle number is not crucial for the filter's performance, and 100 particles are sufficient
38 to represent the high dimensionality of the point-scale system. The frequency of measurements can
39 significantly affect the filter updating performance, and dense ground-based snow observational data
40 always dominate the accuracy of assimilation results. Compared to generic resampling methods, the
41 genetic algorithm used to resample particles can significantly enhance the diversity of particles and
42 prevent particle degeneration and impoverishment. Finally, we concluded that the GPF is a suitable
43 candidate approach for snow data assimilation and is appropriate for different snow climates.

44 **1. Introduction**

45 Understanding snowpack dynamics is crucial for water resource management, agricultural
46 production, avalanche prevention and flood preparedness in snow dominated regions (Piazzini et al.,
47 2019; Pulliainen et al., 2020). As a special land surface type, seasonal snow cover is highly sensitive
48 to climate change and has a significant impact on energy and hydrological processes (Barnett et al.,
49 2005; Takala et al., 2011; Kwon et al., 2017; Che et al., 2014). On one hand, the high albedo of snow-
50 covered surfaces can significantly reduce shortwave radiation absorption, leading to adjustments in
51 the energy exchange between the land surface and atmosphere (You et al., 2020a; You et al., 2020b).
52 On the other hand, the low thermal conductivity of snow cover can insulate the underlying soil, which
53 results in reduced temperature variability and a more stable environment (Zhang et al., 2005; Piazzini
54 et al., 2019). In addition, snowmelt is a vital source of water that plays a critical role in soil moisture,

55 runoff, and groundwater recharge (Dettinger, 2014; Griessinger et al., 2016; Oaida et al., 2019).
56 Therefore, comprehending snow dynamics is essential for predicting snowmelt runoff, atmospheric
57 circulation, hydrological predictions, and climate change.

58 Currently, there is a growing effort to investigate the potential of data assimilation (DA) schemes
59 to improve snow simulations and obtain the optimal posterior estimate of the snowpack state
60 (Bergeron et al., 2016; Piazzi et al., 2018; Smyth et al., 2020; Abbasnezhadi et al., 2021). Various DA
61 methodologies with different degrees of complexity have been developed, resulting in diverse
62 performance levels. Sequential DA techniques, including basic direct insertion, optimal interpolation
63 schemes, ensemble-based Kalman filter, and particle filter, have been widely employed in real-time
64 applications. The greatest strength of sequential DA techniques is that the model state can be
65 sequentially updated when observational data become available (Piazzi et al., 2018). However, the
66 direct insertion method, which replaces model predictions with observations when available, is based
67 on the assumption that the observation is perfect and the model prior is wrong (Malik et al., 2012).
68 This method can potentially result in model shocks due to physical inconsistencies among state
69 variables (Magnusson et al., 2017). Although the optimal interpolation method is more advanced and
70 takes into account observational uncertainty, it still has great limitations and is rarely used in real-
71 time operational systems (Dee et al., 2011; Balsamo et al., 2015).

72 At a higher level are the Kalman filter and ensemble-based Kalman filter, which are most
73 commonly used in various real-time applications. The Ensemble Kalman Filter (EnKF), which was
74 first introduced by Evensen in 2003, uses a Monte Carlo approach to approximate error estimates
75 based on an ensemble of model predictions. This approach does not require model linearization,
76 making it particularly advantageous. Precisely due to this advantage, the EnKF has been widely used
77 in snowpack prediction. For example, EnKF has been used to assimilate MODIS snow cover extent
78 and AMSR-E SWE into a hydrological model to improve modeled SWE (Andreadis et al., 2006), as
79 well as to assimilate MODIS fractional snow cover into a land surface model (Su et al., 2008).
80 Moreover, the EnKF method has been used to enhance snow water equivalent estimation by
81 assimilating ground-based snowfall and snowmelt rates, assimilation of both D-InSAR (Differential
82 Interferometric Synthetic Aperture Radar) and manually measured snow depth data simultaneously
83 (Yang and Li, 2021). Even though there are numerous studies have generally stated that the EnKF
84 has an excellent assimilation performance enabling it to consistently improve snow simulations, some
85 constraining limitations hinder the filter performance (Chen, 2003). One of the main limitations is
86 that the EnKF assumes that the model states follow a Gaussian distribution and only considers the
87 first and second order moments, thereby losing relevant information contained in higher-order
88 moments (Moradkhani et al., 2005). Unfortunately, the dynamical system usually has strong
89 nonlinearity and the involved probability distribution of system state variables is not supposed to
90 follow a Gaussian distribution (Weerts and El Serafy, 2006). Additionally, the filter performance of

91 the EnKF is significantly influenced by the linear updating procedure, and the state-averaging
92 operations can be particularly challenging for highly detailed complex snowpack models.

93 In order to overcome these limitations, the particle filter (PF) which also based on Monte Carlo
94 method has been developed for non-Gaussian, nonlinear dynamic models (Gordon et al., 1993). The
95 greatest strength of PF technique is to be free from the constraints of model linearity and error
96 following a Gaussian distribution. This enables the successful application of the PF technique to
97 nonlinear dynamical systems with non-Gaussian errors. Additionally, the PF technique gives weights
98 to individual particles but leave model states untouched, which makes PF more computationally
99 efficient than the ensemble Kalman filter and smoother techniques (Margulis et al., 2015). Thanks to
100 these advantages, an increasing interest focuses on applying PF technique in snow data assimilation.
101 For example, remotely sensed microwave radiance data were assimilated into a snow model to update
102 model states using the PF technique, and the results demonstrated that the SWE simulations have
103 great improvement (Dechant and Moradkhani, 2011; Deschamps-Berger et al., 2022). A newly PF
104 approach proposed by Margulis et al. (2015) was used to improve SWE estimation through
105 assimilating remotely sensed fractional snow-covered area. At basin scale, PF technique was
106 implemented with the objective of obtaining high resolution retrospective SWE estimates (Cortes et
107 al., 2016). The PF technique was also used to assimilate daily snow depth observations within a multi-
108 layer energy-balance snow model to improve SWE and snowpack runoff simulations (Magnusson et
109 al., 2017). The studies indicated above demonstrated that the assimilated snow-related in-situ
110 measurements or the remotely sensed observation data through the PF technique can successfully
111 update predicted snowpack dynamics, and the PF scheme is a well-performing data assimilation
112 technique enabling to consistently improve model simulations. Nevertheless, particle degeneracy is
113 still a potential limitation of the PF technique. It occurs when most particles have negligible weight,
114 and only a few particles carry significant weights, which hinders a realistic sampling of the underlying
115 probability distribution of the state (Parrish et al., 2012; Abbaszadeh et al., 2017; Abbaszadeh et al.,
116 2018). The particle resampling has been considered to be an efficient approach that can effectively
117 mitigate the problem of particle degeneracy. However, it may result in a sample containing many
118 repeated points and a lack of diversity among the particles, which is referred to as sample
119 impoverishment (Rings et al., 2012; Zhu et al., 2018). And the sample impoverishment was a tricky
120 problem for generic resampling methods. Using intelligent search and optimization methods to
121 mitigate the degeneracy problem may be a good choice because it can effectively avoid sample
122 impoverishment (Park et al., 2009; Ahmadi et al., 2012; Abbaszadeh et al., 2018). The Genetic
123 Algorithm (GA) as an intelligent search and optimization method has been known as an effective
124 approach to mitigate the degeneracy problem and received more attention (Kwok et al., 2005; Park
125 et al., 2009; Mechri et al., 2014). The GA applied in the particle filter, which is referred to as the
126 genetic particle filter (GPF), has been successfully implemented to estimate parameters or states in

127 nonlinear models (Van Leeuwen, 2010; Snyder, 2011). The GPF was also used as data assimilation
128 scheme applied to land surface model which simulates prior subpixel temperature and the results
129 showed the GPF outperformed prior model estimations (Mechri et al., 2014). Despite a series of
130 studies having proven that the GPF is an effective data assimilation approach, however, few studies
131 have investigated the performance of GPF as a snow data assimilation scheme, especially in different
132 snow climates. In view of the promising performances of GPF as a snow data assimilation scheme,
133 this paper aims to investigate the potential of GPF in performing snow data assimilation, and the main
134 goal of this research is to address the following issues: (1) Can the GPF be employed as a snow data
135 assimilation scheme? (2) How is the assimilation performance of GPF in snow data assimilation
136 across different snow climates? (3) The sensitivity of DA simulations to the frequency of the
137 assimilated measurements and the particle number.

138 This paper is organized as follows. Section 2 introduces the study sites, the meteorological
139 dataset, the snow module within the Noah-MP model, the calculation flow of the GPF scheme, and
140 design of the numerical experimental. Section 3 explains the simulation results of SD using the open-
141 loop ensemble, explores the sensitivity of the measurement frequency and ensemble size. Finally,
142 section 4 summarizes the findings of this study.

143 **2. Materials and methods**

144 *2.1 Study sites and data*

145 With consideration of the filtering performance, which may vary in snow climates, eight
146 seasonally snow-covered study sites with different snow climates were selected to implement
147 numerical experimental in this study (Sturm et al., 1995; Trujillo and Molotch, 2014). These sites are
148 distributed at different latitudes in the Northern Hemisphere, and the sites included the Arctic
149 Sodankylä site (SDA, 179 m), located beside the Kitinen River in Finland and the upper 2 meters are
150 frozen (Rautiainen et al., 2014); the Snoqualmie site (SNQ, 921 m) with a rain-snow transitional
151 climate in the Washington Cascades of the USA, the SD measured by snow stakes was employed
152 (Wayand et al., 2015); the maritime Col de Porte (CDP, 1330 m) site in the Chartreuse Range in the
153 Rhone-Alpes region of France; the Mediterranean climate Refugio Poqueira site (ROPA, 2510 m) in
154 Sierra Nevada Mountains of Spain and has a high evaporation rate (Herrero et al., 2009); the
155 Weissfluhjoch site (WFJ, 2540 m) in Davos of Switzerland, and automatic SD observations used in
156 this study (Wever et al., 2015); the continental Swamp Angel Study Plot (SASP, 3370 m) site in the
157 San Juan Mountains of Colorado, USA; and two sites from typical snow-covered regions in China,
158 the Altay meteorological observation site (ATY, 735.3 m) in Northern Xinjiang, China, where there
159 is less wind in the winter season; the other one is the Mohe meteorological observation site (MOHE,
160 438.5 m) in a county of Northeast China, which has a cold temperate continental climate and is the

161 northernmost part of China. Serially complete meteorological measurements are available and can be
 162 used as forcing data in these sites, certainly, the downward longwave and shortwave radiation values
 163 of MOHE were extracted from the China Meteorological Forcing Dataset (CMFD) (Chen et al, 2011),
 164 since there are no radiation measurements in this site.

165 It is noteworthy that the spatial variance of the performance of the model is negligible since
 166 these sites themselves are flat and the surrounding vegetation types are uniform. We have used this
 167 data set to examine the sensitivity of simulated SD to physics options, and the results shown that the
 168 dataset has a reliable quality. In addition, the location, the detailed information of snow climates, and
 169 details about the dataset processing for the eight sites can be also referenced in You et al. (2020a).

170 *2.2 Snow module within Noah-MP model*

171 The snow partial module within Noah-MP model can be divided into up to three layers,
 172 depending on the depth of the snow (Yang et al., 2011). The SD h_{snow} is calculated by

$$173 \quad h_{snow}^t = h_{snow}^{t-1} + \frac{P_{s,g}}{\rho_{sf}} dt . \quad (1)$$

174 where $P_{s,g}$ is the snowfall rate at the ground surface, dt is the timestep, and ρ_{sf} is the bulk
 175 density of the snowfall. When $h_{snow} < 0.025$ m, the snowpack is combined with the top soil layer, and
 176 no dependent snow layer exists. When $0.025 \leq h_{snow} \leq 0.05$ m, a snow layer is created with a thickness
 177 equal to SD. When $0.05 < h_{snow} \leq 0.1$ m, the snowpack will be divided into two layers, each with a
 178 thickness of $\Delta z_{-1} = \Delta z_0 = h_{snow} / 2$. When $0.1 < h_{snow} \leq 0.25$ m, the thickness of the first layer is
 179 $\Delta z_{-1} = 0.05$ m, and the thickness of the second layer is $\Delta z_0 = (h_{snow} - \Delta z_{-1})$ m. When $0.25 < h_{snow} \leq 0.45$ m,
 180 a third layer is created, and the three thickness are: $\Delta z_{-2} = 0.05$ m and $\Delta z_{-1} = \Delta z_0 = (h_{snow} - \Delta z_{-2}) / 2$ m.
 181 When $h_{snow} > 0.45$ m, the layer thickness of the three snow layers are $\Delta z_{-2} = 0.05$ m, $\Delta z_{-1} = 0.2$ m,
 182 $\Delta z_0 = (h_{snow} - \Delta z_{-2} - \Delta z_{-1})$ m. Certainly, the snow cover is highly influenced by air and ground
 183 temperature, and the snow layer combines with the neighboring layer due to sublimation or melting
 184 and is redivided depending on the total SD. The snow module of the Noah-MP model provides an
 185 estimate of snow-related variables using energy and mass balance. This computing process requires
 186 a series of meteorological forcing data, such as near-surface air temperature, precipitation, and
 187 downward solar radiation. The snow accumulation or ablation parameterization of the Noah-MP
 188 model is based on the mass and energy balance of the snowpack, and the snow water equivalent can

189 be calculated using the following equation:

$$190 \quad \frac{dW_s}{dt} = P_{s,g} - M_s - E. \quad (2)$$

191 where W_s is the snow water equivalent (mm), $P_{s,g}$ is the solid precipitation (mm s^{-1}), M_s is the
192 snowmelt rate (mm s^{-1}), E is the snow sublimation rate (mm s^{-1}).

193 A snow interception model was implemented into the Noah-MP model to describe the process
194 of snowfall intercepted by the vegetation canopy (Niu and Yang, 2004). Within this model, the
195 snowfall rate at the ground surface $P_{s,g}$ is then calculated by

$$196 \quad P_{s,g} = P_{s,drip} + P_{s,throu}. \quad (3)$$

197 where $P_{s,drip}$ (mm s^{-1}) is the drip rate of snow and $P_{s,throu}$ (mm s^{-1}) is the through-fall rate of snow. In
198 the Noah-MP model, the ground surface albedo is parameterized as an area-weighted average of the
199 albedos of snow and bare soil, and the snow cover fraction of the canopy is used to calculate the
200 ground surface albedo, as shown in Equation (4),

$$201 \quad \alpha_g = (1 - f_{snow,g}) \alpha_{soil} + f_{snow,g} \alpha_{snow}. \quad (4)$$

202 where α_{soil} and α_{snow} are the albedo of bare soil and snow, respectively. $f_{snow,g}$ is the snow cover
203 fraction on the ground and is parameterized as a function of snow depth, ground roughness length,
204 and snow density (Niu and Yang, 2006).

205 **2.3 Genetic particle filter data assimilation scheme**

206 The Bayesian recursive estimation problem is solved by the Monte Carlo approach within PF
207 technique, making this scheme appropriate for nonlinear system with a non-Gaussian probability
208 distribution (Magnusson et al., 2017). The basic concept of PF technique is to use a large number of
209 randomly generated realizations (i.e., particles) of the system state to represent the posterior
210 distribution. Meanwhile, the particles are propagated forward in time as the model evolves. The
211 weights associated with the particles are updated based on the likelihood of each particle's simulated
212 proximity to the real observation. The weight of the particles can be updated as follows:

$$213 \quad w_t^i = w_{t-1}^i p(z_t | x_t^i). \quad (5)$$

214 where w_{t-1}^i is the weight of i th particle at time $t-1$ and the weight is updated by the likelihood
215 function $p(z_t | x_t^i)$, which measures the likelihood of a given model state with respect to the
216 observation z_t . The observation errors are generally assumed to follow a Gaussian distribution, and

217 the chosen likelihood function represents this assumption. In this study, we employed a normal
218 probability distribution to serve as likelihood function:

$$219 \quad p(z_t | x_t^i) = N(z_t - x_t^i, \sigma). \quad (6)$$

220 where N represents the normal probability distribution of the residuals between observed, z_t , and
221 simulated, x_t . Finally, the weights of the updated model state would be normalized, and the
222 assimilated value of model state is the weighted average of all particles at time t . Although the
223 particle filter has been widely applied in various nonlinear systems, the particle degeneracy and
224 impoverishment in particle filter are still the fatal limitations need to be urgently addressed. To
225 address the degeneration problem in PF technique, traditional resampling methods like multinomial
226 resampling, systematic resampling were employed to resample the particles if the effective sample
227 size,

$$228 \quad N_{eff} = 1 / \sum_{i=1}^N (w_t^i)^2. \quad (7)$$

229 fell below a specified number. Where N is the ensemble size and w_t^i is the normalized weights
230 defined in Equation (5). To be honest, traditional resampling methods can effectively mitigate the
231 problem of particle degeneracy by resampling high-quality particles. However, after multiple
232 iterations, these methods often lead to a serious lack of diversity among particles, which is known as
233 the particle impoverishment problem. To mitigate both of these issues simultaneously, we employed
234 the genetic algorithm (GA) to resample the particles, resulting in the genetic particle filter algorithm
235 (GPF). The GA is inspired by Darwin's theory of evolution and emphasizes the principle of survival
236 of the fittest. In fact, in the resampling phase, the fitness of particles should be reselected according
237 to the theory of particle filtering. Selection, crossover, and mutation are major steps used to simulate
238 population evolution. As shown in Figure 1, these three operators are utilized to produce better
239 offspring and improve the overall population fitness, with the aim of preventing particle degeneracy
240 and impoverishment. These operators will be used to improve particle fitness when it falls below a
241 threshold value. The three operators are described below.

242 **Selection mechanism:** At the time of assimilation, the selection operator will preferentially select the
243 particles that are close to the observed SD. This process is usually achieved by sorting the fitness
244 value of all particles and selecting a certain proportion of particles. Here, we calculated the survival
245 rate of all individuals and sorted them in ascending order. The top fifth percentile of particles were
246 considered high-quality particles and were selected as parents in genetic algorithm. This ensures that
247 fit individuals can be delivered to the next generation group. The survival rate of particles can be
248 calculated using the following equation:

249

$$P(x_{t,i}) = \exp\left[-\frac{1}{R_k}(x_{i,k|k-1} - z_k)^2\right]. \quad (8)$$

250

where R_k is the observation error at time k , 0.01 m was set in this study; z_k represents the

251

observed SD.

252

Crossover mechanism: The purpose of crossover operator is to exchange some genes for two or

253

more chromosomes in a specified way, creating new individuals. GA mainly generates new

254

individuals through this process, which determines the capability of global search. In this study, the

255

arithmetic crossover method was used as the crossover operator to generate new individuals. Two

256

particles were randomly selected from the resampled particle group and combined linearly to form a

257

new particle. Assuming the two selected particles are $\{x_m, x_n\}$, the following equations were used to

258

form the new particles:

259

$$x'_m = \alpha x_m + (1 - \beta) x_n. \quad (9)$$

260

$$x'_n = \beta x_n + (1 - \alpha) x_m. \quad (10)$$

261

where α , β are the empirical crossover coefficients, and $\alpha = 0.45$, $\beta = 0.55$ in this study. In

262

order to ensure diversity among particles, newly formed particles will be discarded when the $x'_m = x'_n$

263

occurred, and parent individuals will be re-selected from the particle group.

264

Mutation mechanism: The mutation in GA refers to replacing the gene values at some loci with

265

other alleles to form a new individual. The mutation mechanism can be considered as a supplement

266

to the crossover mechanism, which can increase the diversity of the population. Assuming that the

267

randomly selected particle from the crossed particle set is x_k , the mutation operation is performed

268

on the particle using the following equation:

269

$$x'_k = x_k + \eta * Uniform. \quad (11)$$

270

where *Uniform* refers a random number from a uniform distribution, η is an empirical coefficient,

271

and 0.01 was set in this study.

272

It is noteworthy that a large number of particles may lead to filter collapse. In this study, we set

273

the number of particles equal to 100 based on previous references (Mechri et al., 2014; Magnusson

274

et al., 2017; Piazzini et al., 2018). Moreover, to prevent the particle ensemble from being unable to

275

represent the prior model state due to structural deficiencies, a Gaussian-type model error, $N(\mu, \sigma)$,

276

was added to the ensemble members. The μ was obtained from the mean value of residual between

277 simulation and observation, and the variance σ was set to 0.01.

278 **2.4 DA experimental design**

279 **2.4.1 Perturbation of meteorological input data**

280 The accuracy of models' output largely depends on the input meteorological forcing dataset for
281 land surface models, and meteorological forcing are one of the major sources of uncertainty affecting
282 simulation results (Raleigh et al., 2015). The precipitation and air temperature are the most important
283 input elements for snow simulations since their roles in determining the quantity of rainfall and
284 snowfall.

285 To produce the forcing data ensemble, the air temperature and precipitation were perturbed
286 following the method of Lei et al. (2014). In this study, the precipitation was assumed to have an error
287 with a log-normal distribution, and it is expressed as follows:

$$288 \quad P_t^i = \exp(\mu_{\ln P} + \varphi_{P,i} \cdot \sigma_{\ln P} / 2). \quad (12)$$

$$289 \quad \sigma_{\ln P} = \sqrt{\ln \left(\frac{(\alpha_p \cdot P_t)^2}{P_t^2} + 1 \right)}. \quad (13)$$

$$290 \quad \mu_{\ln P} = \ln \left(\frac{P_t^2}{\sqrt{P_t^2 + (\alpha_p \cdot P_t)^2}} \right). \quad (14)$$

291 where P_t and P_t^i are the observed and perturbed precipitation at time t , respectively. The log
292 transformation of P_t^i is a Gaussian distribution with a mean ($\mu_{\ln P}$) and a standard deviation ($\sigma_{\ln P}$);
293 α_p is the variance scaling factor of the precipitation, which was set to 0.5 in this study; and $\varphi_{P,i}$ is
294 a normally distributed random number. Meanwhile, the ensemble of the air temperature was obtained
295 as follows:

$$296 \quad T_t^i = T_t - \gamma(1 - 2w^i), w^i \sim U(0,1). \quad (15)$$

297 Where T_t and T_t^i are the observed and perturbed air temperatures at time t , respectively; γ
298 is the variance scaling factor of the temperature with a value of 2.0; and w^i is the random noise with
299 a uniform distribution between 0 and 1. A forcing ensemble containing 100 particles was obtained
300 through above perturbation method in this study.

301 **2.4.2 Evaluation metrics**

302 In order to properly quantify the filter performance, each experiment is evaluated by statistical

303 analysis based on the daily mean values of simulations and observations. In this study, we used the
 304 Kling-Gupta efficiency (KGE) coefficient (Gupta et al., 2009) to evaluate the filter performance,
 305 which allows the analysis of how the assimilation of snow observations succeeds in properly updating
 306 the model simulations, on average:

$$307 \quad KGE = 1 - \sqrt{(r-1)^2 + (a-1)^2 + (b-1)^2}. \quad (16)$$

308 where r is the linear correlation coefficient between the simulated and observed SD; a is the ratio
 309 of the standard deviation of simulated SD to the standard deviation of the observed ones; and b is the
 310 ratio of the mean of simulated SD to the mean of observed ones, here, the simulated SD is the mean
 311 SD ensemble simulations. Theoretically, when $r=1, a=1$ and $b=1$ in Equation (16), the KGE
 312 will obtain the optimal value which equals to 1, and this illustrates that the simulated SD highly
 313 consistently with the observed ones.

314 The time series of SD obtained from assimilation scenarios was compared to observations for
 315 evaluating the performance of the assimilation, and the root-mean-square error (RMSE) was
 316 employed:

$$317 \quad RMSE = \sqrt{\frac{1}{N} \sum_{i=1}^N (obs(i) - sim(i))^2}. \quad (17)$$

318 where N is the total number of observations, $sim(i)$ is the simulated value at time i , and $obs(i)$
 319 is the observed value at time i .

320 Another statistical index is the continuous ranked probability skill score (CRPSS), which is
 321 evaluated to assess changes to the overall accuracy of the ensemble simulations of each experiment
 322 (CRPS) by considering the open-loop ensemble control run as the reference one ($CRPS_{ref}$), and the
 323 calculation scheme is shown in the following formula:

$$324 \quad CRPSS = 1 - \frac{CRPS}{CRPS_{ref}}. \quad (18)$$

325 where CRPS is the continuous ranked probability score which can measure the difference between
 326 continuous probability distribution and deterministic observation samples (detail in Hersbach, 2000).
 327 A smaller CRPS value indicates better probabilistic simulation and the CRPS score of a perfect
 328 simulation would equal to 0. Therefore, the changes in overall accuracy of the SD ensemble
 329 simulations can be measured by CRPSS. However, unlike the CRPS score, the optimal CRPSS score
 330 is equal to 1 and negative values indicate a negative improvement with respect to the reference control
 331 run.

332 **3. Results and discussion**

333 3.1 Open-loop ensemble simulations

334 In order to investigate the impact of meteorological perturbations on snow simulations, an
335 ensemble containing 100 SD simulations derived from as many different meteorological conditions
336 was analyzed. For the sake of concision and clarity, we considered only one winter season for
337 implementing snow simulation experiment at each site, and the results are shown in Figure 2. As
338 shown in Figure 2, the possible overestimation and underestimation of SD simulations produced by
339 the perturbation forcing data were contained within the ensemble spread, which is a direct
340 consequence of the perturbation of the forcing data. Since the meteorological perturbations are
341 unbiased, the physical processes with nonlinear characteristics within the model is supposed to be the
342 main reason for the uncertainty (Piazzini et al. 2018). During the winter season in northern hemisphere,
343 precipitation and air temperature are primary factors that can determine the total amount of snow.

344 As Figure 2 shows, the intervals of SD ensemble are significantly different at different sites,
345 although an identical meteorological perturbation method was used. At some sites, such as ATY,
346 MOHE, WFJ, and CDP, larger SD ensemble spreads were obtained, and most of the SD observations
347 were covered by the ensemble spread. In this case, high-quality particles can be directly selected from
348 the ensemble. However, at some other sites, such as ROPA, SDA, and SASP, narrow SD ensemble
349 spreads were obtained, and the uncertainty interval of simulated SD can hardly cover the observations.
350 In this case, the so-called high-quality particles cannot even be found in the ensemble, and the model
351 prior error becomes a prerequisite for successful assimilation at this time. Especially at the ROPA site,
352 the snow cover was extremely unstable, resulting in difficulty in figuring out any variation rules of
353 SD. The narrow SD ensemble spread at this site also demonstrates that precipitation and air
354 temperature were not the main factors causing snow change. According to the literature, sublimation
355 losses at ROPA ranged from 24% to 33% of total annual ablation and occurred 60% of the time during
356 which snow was present. A high sublimation rate may be the main reason for snow instability (Herrero
357 et al., 2016; You et al., 2020a). This directly leads to a perfect ensemble spread that can cover all
358 observations cannot be produced by perturbing the air temperature and precipitation. Generally
359 speaking, the ensemble produced by perturbing air temperature and precipitation does not contain
360 high-quality particles at this site. It was found that the spread of SD ensembles increases when a
361 snowfall event occurs because the perturbation in precipitation would provide different input snow
362 rates for model realization at all sites. Despite this, we still found that the simulated SD deviated
363 significantly from the observation. For example, at SNQ site, the maximum value of simulated SD
364 was almost half the maximum value of observed SD. In this case, it is impossible to obtain a simulated
365 SD ensemble spread that can cover or nearly cover the observation through perturbing the
366 meteorological forcing data. On the one hand, precipitation and air temperature are not the dominant
367 factors affecting snow cover change, which leads to a narrowed ensemble spread at these sites. On
368 the other hand, although the variation trend of snow cover can be accurately expressed by the Noah-

369 MP model, serious underestimation of the simulated SD shows that the snow simulation performance
370 of Noah-MP is poor at these sites. Nonetheless, the simulated ensembles will be improved whenever
371 the prior error of model state is considered.

372 *3.2 DA simulations with perturbed forcing data*

373 Generally, the ability of a model to simulate autonomously can be limited if observation data is
374 assimilated too frequently, resulting in assimilation results that are essentially the same as the
375 observations and do not reflect the differences among models. To address this, the site's SD
376 measurements were assimilated into the Noah-MP model with an observation frequency of five days
377 in this study, enabling the GPF to perform differently at distinct sites. Figure 3 shows the SD
378 assimilation results across snow climates, indicating a substantial improvement in the SD simulations
379 with satisfactory assimilation performance at all sites. The GPF algorithm can handle not only serious
380 underestimations, such as at SNQ, SDA, but also overestimations during the snow ablation period, as
381 seen at CDP, SASP, ATY, and MOHE sites. These results demonstrate the effectiveness of the GPF
382 algorithm as a snow data assimilation scheme and its ability to significantly improve SD simulations,
383 despite the numerous overestimations and underestimations that may occur in the Noah-MP model's
384 snow simulation results across snow climates.

385 The effectiveness of GPF in updating SD simulations is demonstrated by the KGE values of the
386 DA simulations with perturbed meteorological forcing data, as shown in Figure 4. Although the mean
387 ensemble simulations of SD exhibit substantial improvement at all sites, not all ensemble members
388 were improved, as per the distribution of GPF-DA KGE values. Some ensemble members achieved
389 significant improvement at sites like SDA, SASP, MOHE, and SNQ, while others showed only slight
390 improvement at sites like ATY, WFJ. Figure 4 also reveals that updating SD model simulations at
391 ROPA and WFJ sites is more challenging. Snow simulation performance at the ROPA site is known
392 to be poor due to the high sublimation rate. Certainly, the median value of SD ensemble prediction
393 KGE values is expected to be below zero at this site, indicating that there are few qualified simulations
394 in the prediction ensemble. While the GPF succeeds in enhancing the SD simulations at ROPA, the
395 distribution of GPF-DA KGE values is not concentrated enough, with the 25th percentile
396 approximately at 0.2 and the 75th percentile at about 0.7, indicating that the GPF assimilation
397 algorithm cannot enhance all members but can raise the mean level and obtain an approximation of
398 the optimal posterior estimation. Conversely, the assimilation of snow measurements at CDP site
399 resulted in poor quality of the SD simulations compared to the open-loop ensemble simulations. The
400 median value of GPF-DA KGE was lower than the median value of OL KGE, indicating that a
401 considerable number of ensemble simulations failed to capture the observed values after assimilating
402 snow measurements. However, Figure 3 shows that the mean ensemble simulations after assimilating
403 snow measurements are much closer to SD observations. Thus, it underscores the importance of the
404 ensemble mean in characterizing the filter effectiveness and the approximate value of the optimal

405 posterior estimation of model state. Additionally, the scale of the model ensemble spread was found
406 to be the determinant factor that significantly affects assimilation results. A large ensemble spread
407 can adjust the simulations toward the observed system state even if the model predictions are heavily
408 biased.

409 Figure 5 displays the CRPSS value of GPF-DA at different sites. The smaller the CRPSS value,
410 the worse the probabilistic simulation (with an optimal score of 1). The highest CRPSS score of 0.91
411 was achieved at SASP, while the lowest score of 0.44 was observed at CDP. These results indicate
412 that the GPF enhances the overall accuracy of ensemble simulations most at SASP and least at CDP
413 with respect to the open-loop ensemble simulation. Certainly, this cannot be illustrated by the mean
414 ensemble simulations (Figure 3) but is consistent with the KGE statistical results (Figure 4). Although
415 the open-loop simulations at SNQ exhibited serious underestimation, a satisfactory assimilation result
416 was obtained at this site with a CRPSS score of 0.87. At the SNQ site, the snow simulation
417 performance of Noah-MP model is poor and the model shows serious underestimation during snow
418 stable phase. Implementing a data assimilation experiment in this case is a tricky business since it is
419 difficult to obtain a suitable simulated ensemble by perturbing the meteorological forcings. However,
420 since the model prior error was considered in GPF algorithm, the overall accuracy of the ensemble
421 simulations will be substantially enhanced and this is the reason why a satisfactory assimilation result
422 at SNQ site can be obtained. ROPA was found to be a difficult site to enhance the overall accuracy of
423 ensemble simulations, with a CRPSS score of only 0.58. The snow cover was highly unstable, and
424 the variation of SD exhibited extreme irregularity, which may be the main obstacles to snow data
425 assimilation at this site.

426 Based on these findings, we conclude that the effectiveness of GPF varied among snow climates:
427 it can be employed as a snow data assimilation scheme across snow climates, however, its
428 performance varied across different sites. It is necessary to explore the sensitivity of measurement
429 frequency and ensemble size for the GPF assimilation scheme at various sites.

430 ***3.3 Sensitivity analysis of DA scheme to SD measurement frequency***

431 For complex land/snow process models, model errors can gradually lead to the system deviating
432 from the true value. Therefore, it is necessary to continuously incorporate observations into the model
433 framework to adjust the operating trajectory of the state. Obviously, the frequency of incorporating
434 observations, that is, the assimilation interval, has an important impact on the assimilation system. To
435 investigate the effect of the SD measurement frequency on the performance of GPF, we conducted a
436 sensitivity experiment at eight sites. We aimed to determine how reducing the frequency of SD
437 measurements affects the DA simulations. As expected, a decrease in SD measurement frequency led
438 to a reduction in the impact of the GPF updating on the model simulations, resulting in a gradual
439 increase in the mean RMSE value. Figure 6 illustrates the RMSE ensembles of SD simulations
440 resulting from assimilating different frequency SD measurements over the snow period at each site.

441 Higher frequency SD assimilation improves the accuracy of the simulated SD, as shown by the lower
442 RMSE value achieved when the frequency of SD measurement was set to five days. This means that
443 more frequent SD measurements improve the accuracy of the model, which is particularly useful in
444 regions where snow conditions can change rapidly. The range of RMSE values at different sites varied
445 significantly, as it was related to the maximum value of SD. For instance, a thick snow at SNQ and
446 WFJ sites during the snow period led to larger RMSEs of SD simulations. Notably, an increase in the
447 length of the assimilation window generally resulted in a significant increase in the RMSE value.
448 However, an abnormal occurrence was observed at the SDA site, where the assimilation effect of 20
449 days of SD measurements was significantly better than that of 15 days. Although the RMSE
450 distribution of SD assimilation results with 20 days of observations appeared superior to that of 15
451 days, the RMSE mean values of the two were very close: 0.08 m and 0.07 m, respectively. Therefore,
452 this anomaly can be ignored. These results indicate that the frequency of SD observations has a
453 significant impact on the effectiveness of the GPF algorithm and that a dense amount of observational
454 data can effectively improve the assimilation results.

455 ***3.4 Sensitivity analysis of DA scheme to ensemble size***

456 The results of the experiment aimed at evaluating the impact of particle number on the
457 assimilation performance of GPF are presented in Figure 7. As expected, increasing the particle
458 number up to the threshold leads to a significant improvement in the percent effective sample size.
459 However, the filter performance does not improve significantly when the particle number exceeds the
460 threshold. Figure 7 shows that the GPF algorithm yields the minimum error at all sites when the
461 particle number is set to 100, indicating that one hundred particles can optimize the performance of
462 the GPF algorithm. Although a large particle number can enhance particle diversity and prevent filter
463 divergence, it increases the computation burden without reducing the system error. As illustrated in
464 Figure 7, the RMSEs are generally at the same level when the particle number equals 120 and 160,
465 and they are significantly larger than the RMSE when the particle number is equal to 100. The slight
466 impact of the change in the particle number on the performance of GPF, when the particle number is
467 below the threshold, indicates low system sensitivity to the ensemble size, and this is observed at all
468 sites. Essentially, blindly increasing the particle number does not guarantee a better DA performance
469 of the GPF algorithm. As demonstrated in Figure 7, the RMSEs of simulated snow-depth are virtually
470 unchanged at all sites, despite an increase in the particle number from 120 to 160. This suggests that
471 blindly increasing the ensemble size only increases the computational burden without improving the
472 performance of the GPF.

473 ***3.5 Compared to traditional resampling methods***

474 To demonstrate the effectiveness of using genetic algorithms for particle resampling, we
475 compared the results of our genetic algorithm (PF-G) to those of traditional resampling methods:

476 systematic resampling (PF-S) and multinomial resampling (PF-M), which are both commonly used
477 in particle resampling. The calculation process for these methods is detailed in the particle filter
478 introduction references. Figure 8 shows the RMSE values for SD simulations obtained using these
479 three methods. We found that the PF-G outperforms PF-M and PF-S at all sites, as evidenced by the
480 significantly smaller mean and median RMSE values. This indicates that the PF-G is suitable for
481 snow data assimilation in various snow climates and is somewhat superior to traditional particle filters.
482 At most sites (MOHE, ATY, SDA, and ROPA), PF-M and PF-S showed similar performance, meaning
483 that these methods did not produce a significant difference in the assimilation results. This is because
484 these traditional resampling methods can only mitigate particle degeneration by resampling particles,
485 but are unable to prevent particle impoverishment. Therefore, they are unable to select high-quality
486 particles and keep the particles have variety. Significantly, the mean and median RMSE values for
487 PF-G were lower than those of PF-M and PF-S at several sites (SASP, SNQ, and WFJ) where the
488 snow cover was relatively thick, with maximum SD during the snow period reaching 2.45 m, 2.95 m,
489 and 2.40 m, respectively. This suggests that PF-G performs better in assimilating data from thick
490 snow covers.

491 The multinomial and systematic resampling methods select particles from the original particle
492 set at different levels or based on the accumulation of particle weights. Both of the resampling
493 methods extract particles from the entire particle set, and the corresponding particle values do not
494 undergo any essential changes. However, when compared to the two traditional particle resampling
495 methods, the genetic algorithm first uses the fitness function to calculate the "survival rate" of each
496 particle one by one, and then performs crossover, mutation and other operations on the selected
497 particles. This approach ensures that the resampled particles are high-quality particles, which is the
498 main reason why genetic particle filtering has an advantage in the snow data assimilation experiments.
499 As Figure 8 shows, the assimilation error of the genetic particle filter is the smallest at all sites. From
500 the results of the real assimilation experiment, it can be seen that genetic particle filtering has more
501 advantages over the other two methods.

502 **4. Conclusions**

503 In this study, we investigated the potential of using GPF as a snow data assimilation scheme
504 across eight sites with varying snow climates. We addressed the problem of degeneration and
505 impoverishment in PF algorithm by using the genetic algorithm to resample particles. We also
506 examined the sensitivity of GPF scheme to measurement frequency and ensemble size. The main
507 findings of this study are as follows:

- 508 1. The GPF was an effective snow data assimilation scheme and can be used across different snow
509 climates. The genetic algorithm effectively addressed the problem of particle degeneration and

510 impoverishment in the PF algorithm.

511 2. Our experiment showed that the system has low sensitivity to the particle number, and 100
512 particles can achieve a better assimilation result across different snow climates. This indicates
513 that 100 particles are suitable for representing the high dimensionality of the system.

514 3. We found that perturbations in meteorological forcing data were not sufficient to provide
515 ensemble spread, resulting in poor filter performance. Particle inflation can make up for this
516 deficiency. Moreover, we observed that the RMSE of simulated SD decreased significantly with
517 the increase of the frequency of SD measurement, indicating that dense observational data can
518 improve the assimilation results.

519 4. Compared to the two classic resampling methods, the particle filter with genetic algorithm as
520 resampling method shows a better assimilation performance especially in a thick snow cover, the
521 distributed RMSEs are more centralized and a smaller mean error will be obtained.

522 Our experiments were based on forcing data and snow observations from various sites with different
523 snow climates. While our results provide a reference for applying GPF to snow data assimilation,
524 further research is needed to investigate the performance of GPF on a regional scale and to explore
525 the assimilation of snow observational data from remote sensing or wireless sensor networks into
526 land surface models using GPF. In summary, our study demonstrates the feasibility of using GPF for
527 snow data assimilation and provides valuable insights for future research in this area.

528 **Acknowledgements**

529 Our research received support from several sources, including the National Natural Science
530 Foundation of China (grant number 42101361, 42130113, 41871251, and 41971326), the Scientific
531 research project of higher education institutions in Anhui province, and the Key Research and
532 Development Program of Anhui Province (2022107020028).

533 **References**

- 534 Abbasnezhadi, K., Rousseau, A. N., Foulon, E., and Savary, S.: Verification of regional deterministic
535 precipitation analysis products using snow data assimilation for application in meteorological
536 network assessment in sparsely gauged Nordic basins, *Journal of Hydrometeorology*, 22, 859-
537 876, <https://doi.org/10.1175/JHM-D-20-0106.1>, 2021.
- 538 Abbaszadeh, P., Moradkhani, H., Yan, H. X.: Enhancing hydrologic data assimilation by evolutionary
539 particle filter and Markov Chain Monte Carlo, *Advances in Water Resources*, 111, 192-204,
540 <https://doi.org/10.1016/j.advwatres.2017.11.011>, 2018.
- 541 Ahmadi, M., Mojallali, H., Izadi-Zamanabadi, R.: State estimation of nonlinear stochastic systems
542 using a novel meta-heuristic particle filter, *Swarm and Evolutionary Computation*, 4, 44-53,
543 <https://doi.org/10.1016/j.swevo.2011.11.004>, 2012.

- 544 Andreadis, K. M., Lettenmaier, D. P.: Assimilating remotely sensed snow observations into a
545 macroscale hydrology model, *Advances in water resources*, 29, 872-886, [https://doi.org/](https://doi.org/10.1016/j.advwatres.2005.08.004)
546 10.1016/j.advwatres.2005.08.004, 2006.
- 547 Barnett, T. P., Adam, J. C., Lettenmaier, D. P.: Potential impacts of a warming climate on water
548 availability in snow-dominated regions, *Nature*, 438, 303-309, [https://doi.org/](https://doi.org/10.1038/nature04141)
549 10.1038/nature04141, 2005.
- 550 Balsamo, G., Albergel, C., Beljaars, A., Boussetta, S., Burun, E., Cloke, H., Dee, D., Dutra, E.,
551 Munoz-Sabater, J., Pappenberger, F., de Rosnay, P., Stockdale, T., and Vitart, F.: ERA-
552 Interim/Land: a global land surface reanalysis data set, *Hydrology and Earth System Sciences*,
553 19, 389-407, <https://doi.org/10.5194/hess-19-389-2015>, 2015.
- 554 Bergeron, J. M., Trudel, M., Leconte, R.: Combined assimilation of streamflow and snow water
555 equivalent for mid-term ensemble streamflow forecasts in snow-dominated regions, *Hydrology*
556 *and Earth System Sciences*, 20, 4375-4389, <https://doi.org/10.5194/hess-20-4375-2016>, 2016.
- 557 Che, T., Li, X., Jin, R., and Huang, C. L.: Assimilating passive microwave remote sensing data into a
558 land surface model to improve the estimation of snow depth, *Remote Sensing of Environment*,
559 143, 54-63, <https://doi.org/10.1016/j.rse.2013.12.009>, 2014.
- 560 Chen, Z.: Bayesian filtering: From Kalman filters to particle filters, and beyond, *Adaptive Systems*
561 *Laboratory Technical Report*, McMaster University, Hamilton, 25pp., 2003.
- 562 Chen, Y. Y., Yang, K., He, J., Qin, J., Shi, J. C., Du, J. Y., and He, Q.: Improving land surface
563 temperature modeling for dry land of China, *Journal of Geophysical Research-Atmospheres*,
564 116, D20104, <https://doi.org/10.1029/2011JD015921>, 2011.
- 565 Cortes, G., Giroto, M., Margulis, S.: Snow process estimation over the extratropical Andes using a
566 data assimilation framework integrating MERRA data and Landsat imagery, *Water Resources*
567 *Research*, 52, 2582-2600, <https://doi.org/10.1002/2015WR018376>, 2016.
- 568 Dee, D. P., Uppala, S. M., Simmons, A. J., Berrisford, P., Poli, P., Kobayashi, S., Andrae, U.,
569 Balmaseda, M. A., Balsamo, G., Bauer, P., Bechtold, P., Beljaars, A. C. M., van de Berg, L.,
570 Bidlot, J., Bormann, N., Delsol, C., Dragani, R., Fuentes, M., Geer, A. J., Haimberger, L., Healy,
571 S. B., Hersbach, H., Holm, E. V., Isaksen, L., Kallberg, P., Koehler, M., Matricardi, M., McNally,
572 A. P., Monge-Sanz, B. M., Morcrette, J. J., Park, B. -K., Peubey, C., de Rosnay, P., Tavolato, C.,
573 Thepaut, J. N., and Vitart, F.: The ERA-Interim reanalysis: configuration and performance of the
574 data assimilation system, *Quarterly Journal of the Royal Meteorological Society*, 137, 553-597,
575 <https://doi.org/10.1002/qj.828>, 2011.
- 576 Dechant, C., Moradkhani, H.: Radiance data assimilation for operational snow and streamflow
577 forecasting, *Advances in Water Resources*, 34, 351-364, [https://doi.org/](https://doi.org/10.1016/j.advwatres.2010.12.009)
578 10.1016/j.advwatres.2010.12.009, 2011.
- 579 Deschamps-Berger, C., Cluzet, B., Dumont, M., Lafaysse, M., Berthier, E., Fanise, P., Gascoin, S.:
580 Improving the Spatial Distribution of Snow Cover Simulations by Assimilation of Satellite
581 Stereoscopic Imagery, *Water Resources Research*, 58, <https://doi.org/10.1029/2021WR030271>,
582 2022.
- 583 Dettinger, M.: Climate change impacts in the third dimension, *Nature Geoscience*, 7, 166-167,

584 <https://doi.org/10.1038/ngeo2096>, 2014.

585 Evensen, G.: The ensemble Kalman filter: Theoretical formulation and practical implementation,
586 *Ocean Dynamics*, 53, 343-367, <https://doi.org/10.1007/s10236-003-0036-9>, 2003.

587 Gelb, A.: Optimal linear filtering, in: Applied optimal estimation, MIT Press, Cambridge, Mass, 102-
588 155, 1974.

589 Gordon, N. J., Salmond, D. J., Smith, A. F. M.: Novel-Approach to nonlinear non-Gaussian bayesian
590 state estimation, *IEE Proceedings-F Radar and Signal Processing*, 140, 107-113, <https://doi.org/10.1049/ip-f-2.1993.0015>, 1993.

592 Griessinger, N., Seibert, J., Magnusson, J., and Jonas, T.: Assessing the benefit of snow data
593 assimilation for runoff modeling in Alpine catchments, *Hydrology and Earth System Sciences*,
594 20, 3895-3905, <https://doi.org/10.5194/hess-20-3895-2016>, 2016.

595 Gupta, H. V., Kling, H., Yilmaz, K. K., and Martinez, G. F.: Decomposition of the mean squared error
596 and NSE performance criteria: Implications for improving hydrological modelling, *Journal of*
597 *Hydrology*, 377, 80-91, <https://doi.org/10.5194/10.1016/j.jhydrol.2009.08.003>, 2009.

598 Herrero, J., Polo, M. J., Monino, A., and Losada, M. A.: An energy balance snowmelt model in a
599 Mediterranean site, *Journal of Hydrology*, 371, 98-107, <https://doi.org/10.1016/j.jhydrol.2009.03.021>, 2009.

601 Herrero, J., Polo, M. J., Pimentel, R., and Pérez-Palazón, M. J.: Meteorology and snow depth at
602 Refugio Poqueira (Sierra Nevada, Spain) at 2510 m 2008-2015, PANGEA, 2016.

603 Hersbach, H.: Decomposition of the continuous ranked probability score for ensemble prediction
604 systems, *Weather and Forecasting*, 15, 559-570, [https://doi.org/10.1175/1520-0434\(2000\)015<0559:DOTCRP>2.0.CO;2](https://doi.org/10.1175/1520-0434(2000)015<0559:DOTCRP>2.0.CO;2), 2000.

606 Kwok, N., Fang, G., Zhou, W.: Evolutionary particle filter: resampling from the genetic algorithm
607 perspective. In: *Proceedings of International Conference on Intelligent Robots and Systems*,
608 Shaw Conference Centre, Edmonton, Alberta, Canada, August 2-6, pp. 2935-2940, 2005.

609 Kwon, Y., Yang, Z. L., Hoar, T. J., and Toure, A. M.: Improving the radiance assimilation performance
610 in estimating snow water storage across snow and land-cover types in North America, *Journal*
611 *of Hydrometeorology*, 18, 651-668, <https://doi.org/10.1175/JHM-D-16-0102.1>, 2017.

612 Lei, F. N., Huang, C. L., Shen, H. F., and Li, X.: Improving the estimation of hydrological states in
613 the SWAT model via the ensemble Kalman smoother: Synthetic experiments for the Heihe River
614 Basin in northwest China, *Advances in Water Resources*, 67, 32-45, <https://doi.org/10.1016/j.advwatres.2014.02.008>, 2014.

616 Malik, M. J., van der Velde, R., Vekerdy, Z., and Su, Z. B.: Assimilation of Satellite-Observed Snow
617 Albedo in a Land Surface Model, *Journal of Hydrometeorology*, 13, 1119-1130, <https://doi.org/10.1175/JHM-D-11-0125.1>, 2012.

619 Magnusson, J., Gustafsson, D., Husler, F., and Jonas, T.: Assimilation of point SWE data into a
620 distributed snow cover model comparing two contrasting methods, *Water Resources Research*,
621 50, 7816-7835, <https://doi.org/10.1002/2014WR015302>, 2014.

- 622 Margulis, S. A., Giroto, M., Cortes, G., and Durand, M.: A particle batch smoother approach to snow
623 water equivalent estimation, *Journal of Hydrometeorology*, 16, 1752-1772, [https://doi.org/](https://doi.org/10.1175/JHM-D-14-0177.1)
624 10.1175/JHM-D-14-0177.1, 2015.
- 625 Magnusson, J., Winstral, A., Stordal, A. S., Essery, R., and Jonas, T: Improving physically based snow
626 simulations by assimilating snow depths using the particle filter, *Water Resources Research*, 53,
627 1125-1143, <https://doi.org/10.1002/2016WR019092>, 2017.
- 628 Moradkhani, H., Hsu, K. L., Gupta, H., and Sorooshian, S.: Uncertainty assessment of hydrologic
629 model states and parameters: Sequential data assimilation using the particle filter, *Water*
630 *Resources Research*, 41, W05012, <https://doi.org/10.1029/2004WR003604>, 2005.
- 631 Mechri, R., Otle, C., Pannekoucke, O., and Kallel, A.: Genetic particle filter application to land
632 surface temperature downscaling, *Journal of Geophysical Research-Atmospheres*, 119, 2131-
633 2146, <https://doi.org/10.1002/2013JD020354>, 2014.
- 634 Niu, G. Y., Yang, Z. L.: Effects of vegetation canopy processes on snow surface energy and mass
635 balances, *Journal of Geophysical Research-Atmospheres*, 109, D23111, [https://doi.org/](https://doi.org/10.1029/2004JD004884)
636 10.1029/2004JD004884, 2004.
- 637 Niu, G. Y., Yang, Z. L.: Effects of frozen soil on snowmelt runoff and soil water storage at a
638 continental scale, *Journal of Hydrometeorology*, 7, 937-952, <https://doi.org/10.1175/JHM538.1>,
639 2006.
- 640 Oaida, C. M., Reager, J. T., Andreadis, K. M., David, C. H., Levoe, S. R., Painter, T. H., Bormann, K.
641 J., Trangsrud, A. R., Giroto, M., and Famiglietti, J. S.: A high-resolution data assimilation
642 framework for snow water equivalent estimation across the western United States and validation
643 with the airborne snow observatory, *Journal of Hydrometeorology*, 20, 357-378,
644 <https://doi.org/10.1175/JHM-D-18-0009.1>, 2019.
- 645 Park, S., Hwang, J. P., Kim, E., and Kang, H. J.: A new evolutionary particle filter for the prevention
646 of sample impoverishment, *IEEE Transaction on Evolutionary Computation*, 13, 801-809,
647 <https://doi.org/10.1109/TEVC.2008.2011729>, 2009.
- 648 Parrish, M. A., Moradkhani, H., DeChant, C. M.: Toward reduction of model uncertainty: Integration
649 of Bayesian model averaging and data assimilation, *Water Resources Research*, 48, W03519,
650 <https://doi.org/10.1029/2011WR011116>, 2012.
- 651 Piazzzi, G., Campo, L., Gabellani, S., Castelli, F., Cremonese, E., di Cella, U. M., Stevenin, H., and
652 Ratto, S. M.: An EnKF-based scheme for snow multivariable data assimilation at an Alpine site,
653 *Journal of Hydrology and Hydromechanics*, 67, 4-19, <https://doi.org/10.2478/joh-h-2018-0013>,
654 2019.
- 655 Piazzzi, G., Thirel, G., Campo, L., and Gabellani, S.: A particle filter scheme for multivariate data
656 assimilation into a point-scale snowpack model in an Alpine environment, *Cryosphere*, 12, 2287-
657 2306, <https://doi.org/10.5194/tc-12-2287-2018>, 2018.
- 658 Pulliainen, J., Luojus, K., Derksen, C., Mudryk, L., Lemmetyinen, J., Salminen, M., Ikonen, J., Takala,
659 M., Cohen, J., Smolander, T., and Norberg, J.: Patterns and trends of Northern Hemisphere snow
660 mass from 1980 to 2018, *Nature*, 581, 294-298, <https://doi.org/10.1038/s41586-020-2258-0>,
661 2020.

- 662 Rautiainen, K., Lemmetyinen J., Schwank, M., Kontu, A., Menard, C. B., Matzler, C., Drusch, M.,
663 Wiesmann, A., Ikonen, J., and Pulliainen, J.: Detection of soil freezing from L-band passive
664 microwave observations, *Remote Sensing of Environment*, 147, 206-218, <https://doi.org/10.1016/j.rse.2014.03.007>, 2014.
- 666 Raleigh, M. S., Lundquist, J. D., Clark, M.P.: Exploring the impact of forcing error characteristics on
667 physically based snow simulations within a global sensitivity analysis framework, *Hydrology
668 and Earth System Sciences*, 19, 3153-3179, <https://doi.org/10.5194/hess-19-3153-2015>, 2015.
- 669 Rings, J., Vrugt, J. A., Schoups, G., Huisman, J. A., and Vereecken, H.: Bayesian model averaging
670 using particle filtering and Gaussian mixture modeling: Theory, concepts, and simulation
671 experiments, *Water Resources Research*, 48, W05520, <https://doi.org/10.1029/2011WR011607>,
672 2012.
- 673 Smyth, E. J., Raleigh, M. S., Small, E. E.: Improving SWE estimation with data assimilation: the
674 influence of snow depth observation timing and uncertainty, *Water Resources Research*, 56,
675 e2019WR026853, <https://doi.org/10.1029/2019WR026853>, 2020.
- 676 Sturm, M., Holmgren, J., Liston, G. E.: A seasonal snow cover classification system for local to global
677 applications, *Journal of Climate*, 8, 1261-1283, [https://doi.org/10.1175/1520-0442\(1995\)008<1
678 261:ASSCCS>2.0.CO;2](https://doi.org/10.1175/1520-0442(1995)008<1261:ASSCCS>2.0.CO;2), 1995.
- 679 Su, H., Yang, Z. L., Niu, G. Y., and Dickinson, R. E.: Enhancing the estimation of continental-scale
680 snow water equivalent by assimilating MODIS snow cover with the ensemble Kalman filter,
681 *Journal of Geophysical Research-Atmospheres*, 113, D08120, [https://doi.org/10.1029/2007JD00
682 9232](https://doi.org/10.1029/2007JD009232), 2008.
- 683 Snyder, C.: Particle filters, the optimal proposal and high-dimensional systems, *ECMWF Seminar on
684 Data Assimilation for Atmosphere and Ocean*, pp. 6-9, Reading, U. K., 2011.
- 685 Takala, M., Luojus, K., Pulliainen, J., Derksen, C., Lemmetyinen, J., Karna, J. P., Koskinen, J., and
686 Bojkov, B.: Estimating northern hemisphere snow water equivalent for climate research through
687 assimilation of space-borne radiometer data and ground-based measurements, *Remote Sensing
688 of Environment*, 115, 3517-3529, <https://doi.org/10.1016/j.rse.2011.08.014>, 2011.
- 689 Trujillo, E., Molotch, N.P.: Snowpack regimes of the Western United States, *Water Resources
690 Research*, 50, 5611-5623, <https://doi.org/10.1002/2013WR014753>, 2014.
- 691 Van Leeuwen, P. J.: Nonlinear data assimilation in geosciences: An extremely efficient particle filter,
692 *Quarterly Journal of the Royal Meteorological Society*, 136, 1991-1999, [https://doi.org/
693 10.1002/qj.699](https://doi.org/10.1002/qj.699), 2010.
- 694 Wayand, N. E., Massmann, A., Butler, C., Keenan, E., Stemberis, J., and Lundquist, J. D.: A
695 meteorological and snow observational data set from Snoqualmie Pass (921 m), Washington
696 Cascades, USA, *Water Resources Research*, 51, 10092-10103, [https://doi.org/10.1002/2015WR
697 017773](https://doi.org/10.1002/2015WR017773), 2015.
- 698 Weerts, A. H., El Serafy, G. Y. H.: Particle filtering and ensemble Kalman filtering for state updating
699 with hydrological conceptual rainfall-runoff models, *Water Resources Research*, 42, W09403,
700 <https://doi.org/10.1029/2005WR004093>, 2006.

701 Wever, N., Schmid, L., Heilig, A., Eisen, O., Fierz, C., and Lehning, M.: Verification of the multi-
702 layer SNOWPACK model with different water transport schemes, *The Cryosphere*, 9, 2271-
703 2293, <https://doi.org/10.5194/tc-9-2271-2015>, 2015.

704 Yang, J. M., Li, C. Z.: Assimilation of D-InSAR snow depth data by an ensemble Kalman filter,
705 *Arabian Journal of Geosciences*, 14, 1-14, <https://doi.org/10.1007/s12517-021-06699-y>, 2021.

706 You, Y. H., Huang, C. L., Yang, Z. L., Zhang, Y., Bai, Y. L., and Gu, J.: Assessing Noah-MP
707 parameterization sensitivity and uncertainty interval across snow climates, *Journal of*
708 *Geophysical Research-Atmospheres*, 125, e2019JD030417, [https://doi.org/10.1029/2019JD030](https://doi.org/10.1029/2019JD030417)
709 417, 2020.

710 Zhang, T. J.: Influence of the seasonal snow cover on the ground thermal regime: An overview,
711 *Reviews of Geophysics*, 43, RG4002, <https://doi.org/10.1029/2004RG000157>, 2005.

712 Zhu, G. F., Li, X., Ma, J.Z., Wang, Y. Q., Liu, S. M., Huang, C. L., Zhang, K., and Hu, X. L.: A new
713 moving strategy for the sequential Monte Carlo approach in optimizing the hydrological model
714 parameters, *Advances in Water Resources*, 114, 164-179, [https://doi.org/10.1016/j.advwatres.](https://doi.org/10.1016/j.advwatres.2018.02.007)
715 2018.02.007, 2018.

716

717

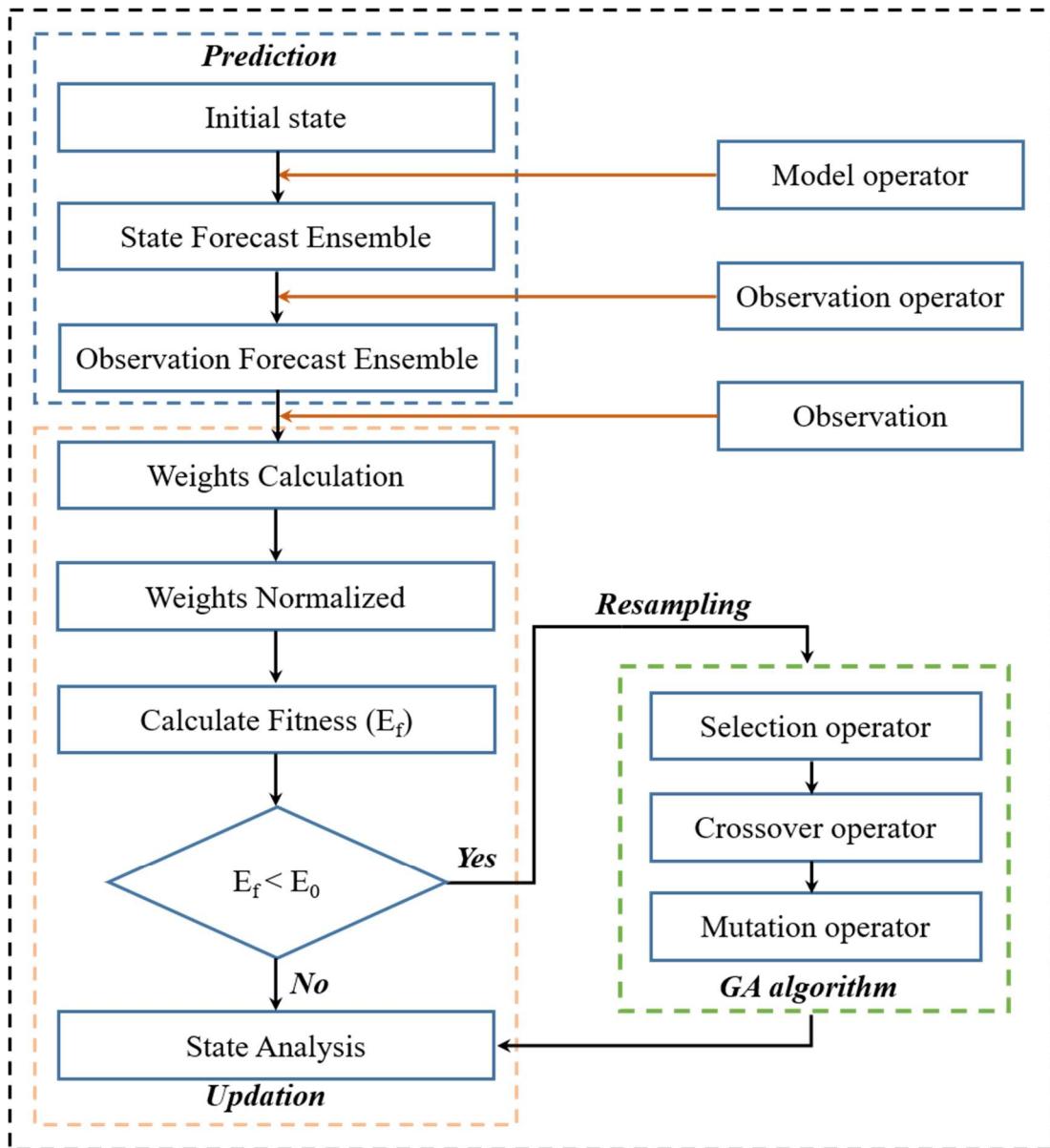
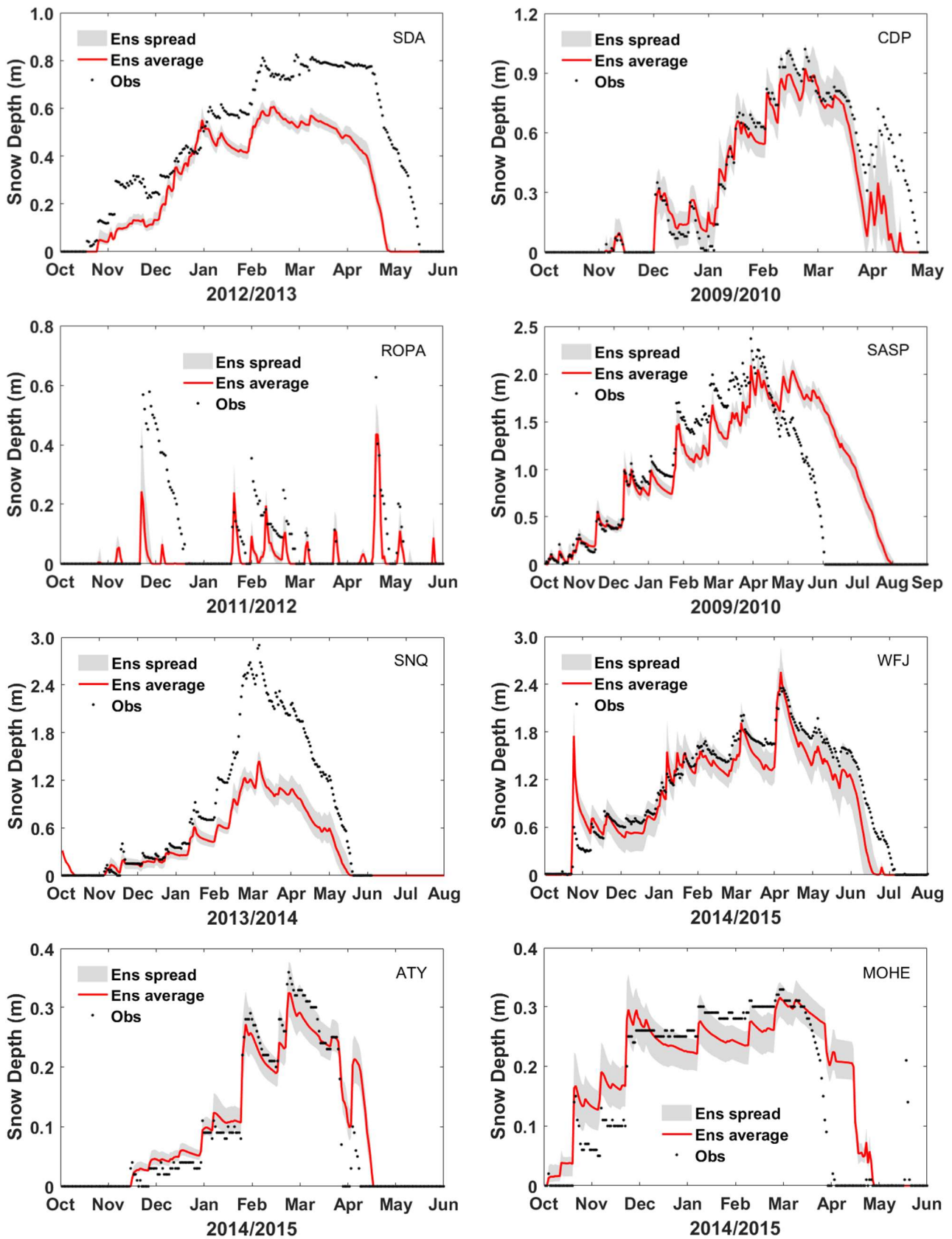


Figure 1. Flowchart of Genetic particle filter

718

719

720

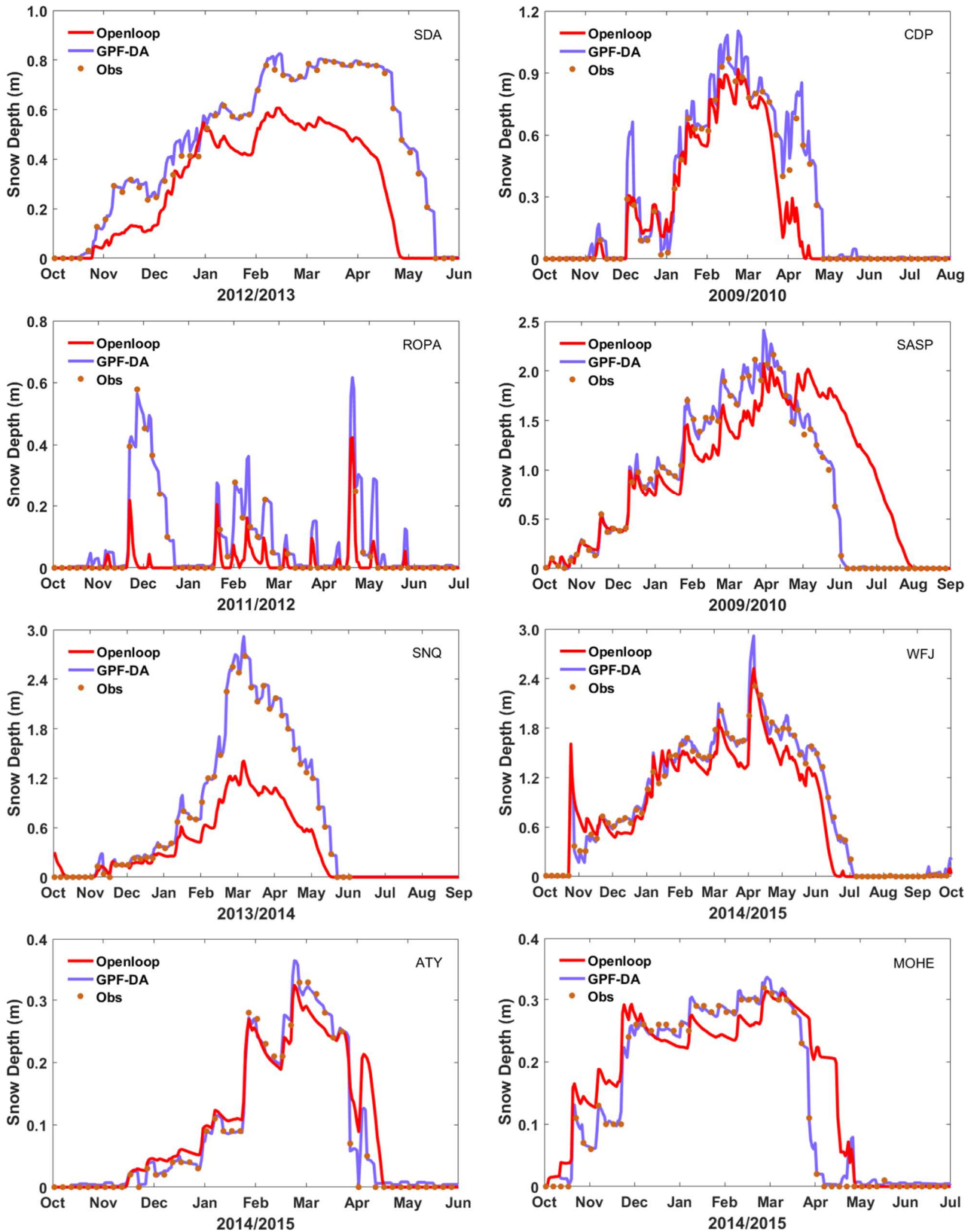


721

722

723

Figure 2. Impact of the meteorological uncertainty on snow depth ensemble simulations

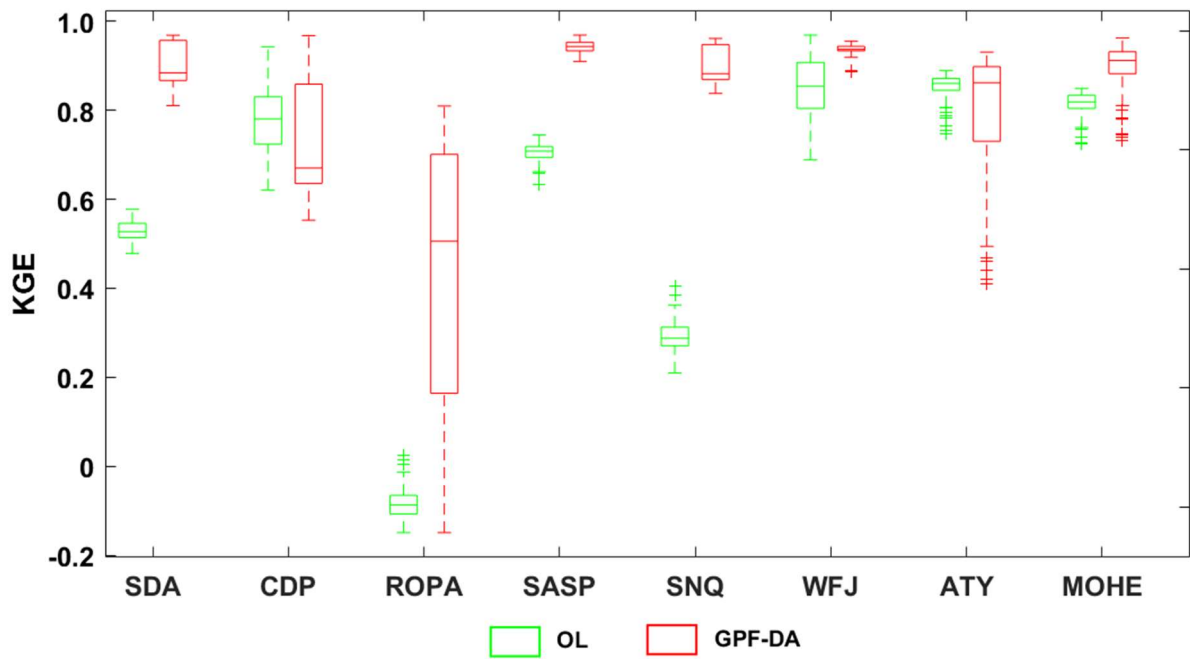


724

725 **Figure 3.** Evaluation of the SD at eight sites from mean ensemble simulation and assimilation with
 726 the measurements.

727

728

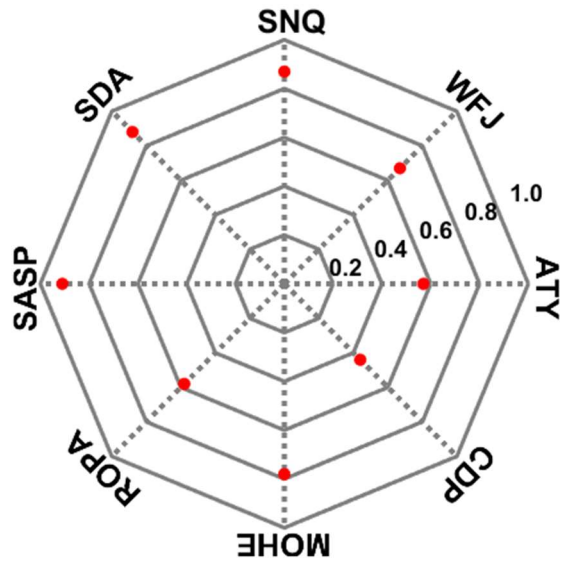


729

730 **Figure 4.** The KGE values of SD simulations, the OL and GPF-DA are in green, red, respectively.

731 The bottom and top edges of each box indicate the 25th 75th percentiles, respectively. The line in the
 732 middle of each box is the median.

733

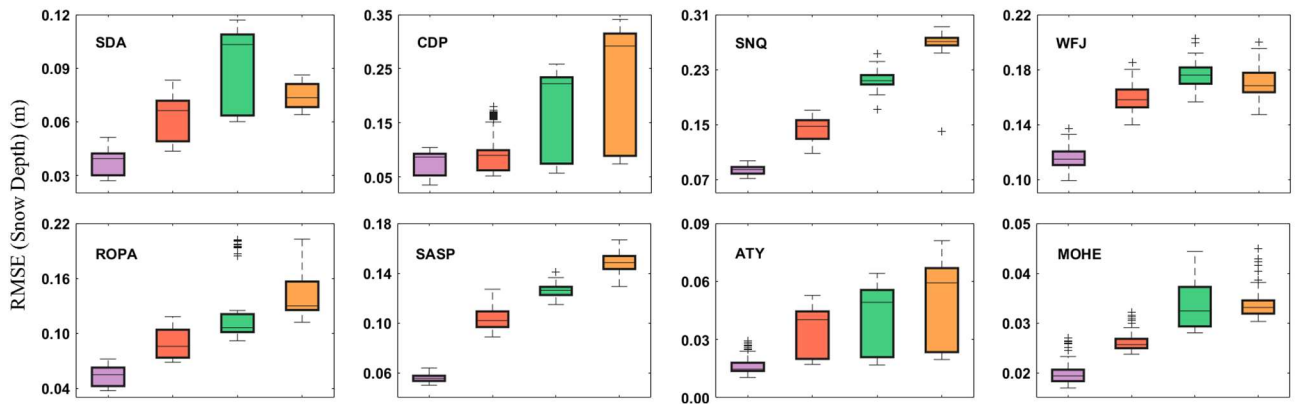


734

735

Figure 5. Comparison of the CRPSS value of GPF-DA at different sites.

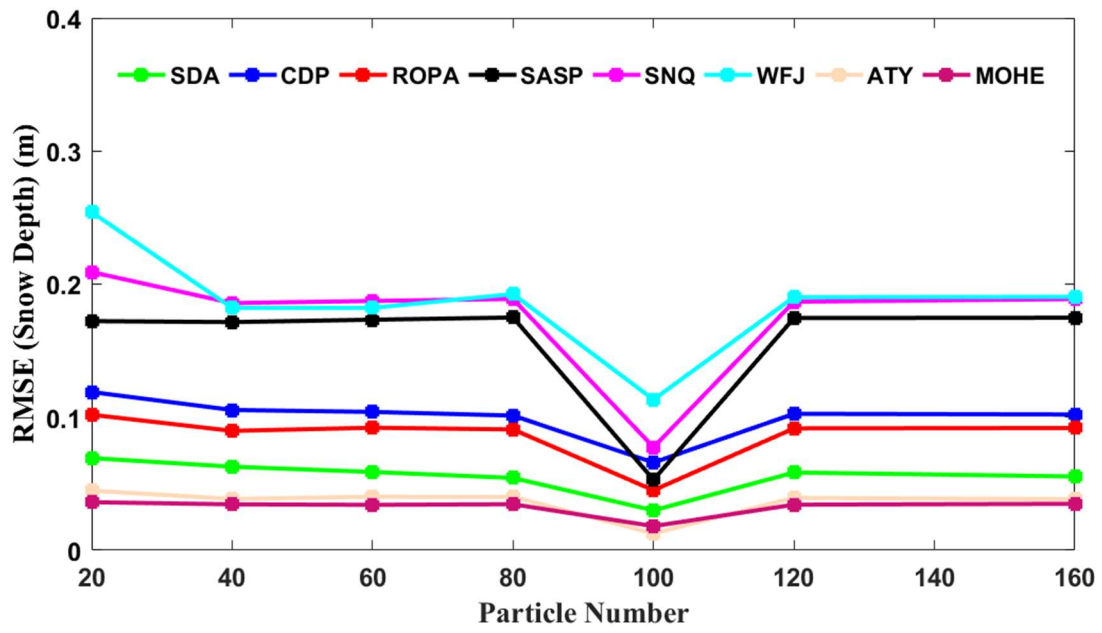
736



737

738 **Figure 6.** The RMSE values of SD simulations at different sites, from left to right in each subfigure
 739 are the assimilation observation frequency is 5, 10, 15, 20 days, respectively, and with different colors.

740

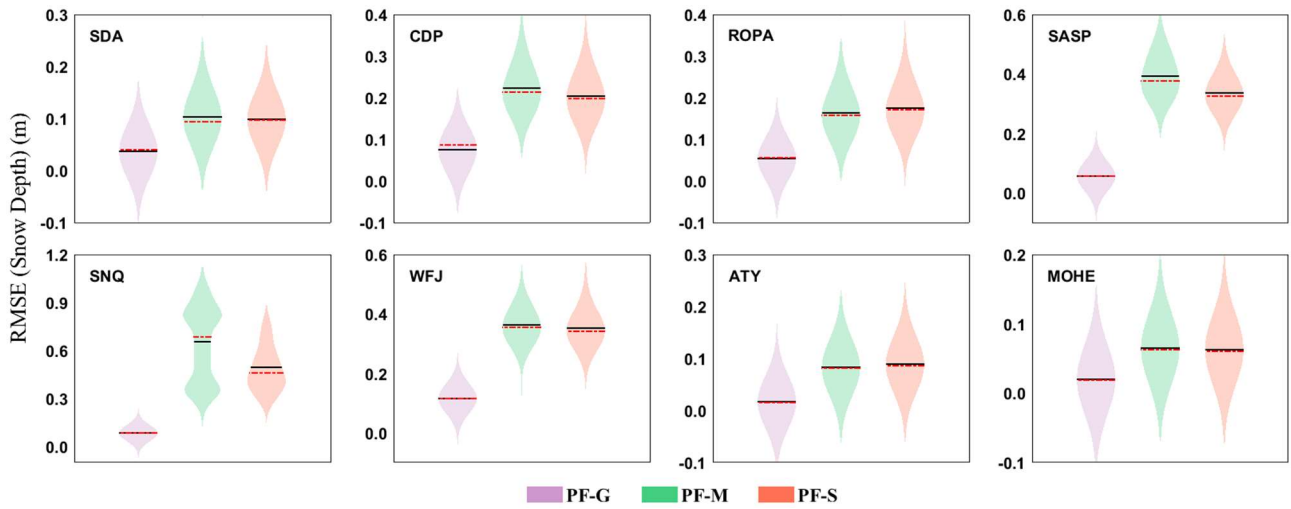


741

742 **Figure 7.** Sensitivity analysis of the GPF snow DA scheme to particle number at eight sites, during

743 different snow periods.

744



745

746 **Figure 8.** The RMSE values of SD simulations by three different resampling methods. For each
 747 subfigure, from left to right are the particles resampled by genetic algorithm, multinomial method,
 748 systematic method, respectively, and with different colors, the black line indicates the mean, and the
 749 red line indicates the median; the kernel bandwidth was 0.05.

750